coatings

MDPI

Article

Dual-Scale Femtosecond-Laser Stripe Microstructures Regulate Fibroblast Behavior for Functional Soft-Tissue Control on Titanium Mesh Implants

Jiaru Zhang [1], Tao Yu [2], Xinran Zhang [3], Jin Yang [3] and Libin Lu [4,*]

[1] School of Mechanical and Automotive Engineering, Ningbo University of Technology, Ningbo 315336, China
[2] Department of Stomatology, Ningbo Beilun District People's Hospital, Ningbo 315826, China
[3] Ningbo Hangzhou Bay Branch, Zhejiang Jirun Automobile Co., Ltd., Ningbo 315336, China
[4] Ningbo Institute of Technology, Beihang University, Ningbo 315832, China
* Correspondence: lulibin@buaa.edu.cn

Abstract

Soft-tissue management is critical for guided bone regeneration (GBR), yet conventional titanium meshes lack the ability to regionally regulate fibroblast behavior where opposite biological responses are needed. Here, we fabricated two femtosecond-laser patterned stripe topographies on titanium using a unidirectional scanning strategy with parameter tuning, generating LSFL with a periodicity of 820 ± 30 nm and micro-grooves with a periodicity of 4.7 ± 0.1 µm. Surface morphology and physicochemical properties were characterized by SEM/AFM, XPS, microhardness testing, and wettability measurements. Human gingival fibroblasts (HGF-1) were used to assess adhesion, cytoskeletal organization, spreading area, and proliferation (CCK-8). The submicron LSFL promoted robust fibroblast adhesion, aligned cytoskeletal organization, larger spreading areas, and higher proliferation, whereas the micro-groove surface markedly restricted spreading and was associated with poorer cytoskeletal organization and lower proliferation. Alternating patterned regions further demonstrated geometry-driven spatial selectivity, with preferential cell occupation on LSFL stripes. These findings support a fabrication-ready surface-engineering strategy to synchronize rapid soft-tissue sealing while restricting unwanted fibroblast advancement at defined regions, offering a promising route toward more predictable GBR outcomes.

Keywords: femtosecond laser; laser-induced periodic surface structures (LIPSS); dual-function interface; titanium mesh; human gingival fibroblasts (HGF-1)

Check for updates

Academic Editor: James Kit-Hon Tsoi

Received: 26 January 2026
Revised: 18 February 2026
Accepted: 24 February 2026
Published: 26 February 2026

Copyright: © 2026 by the authors. Licensee MDPI, Basel, Switzerland. This article is an open access article distributed under the terms and conditions of the Creative Commons Attribution (CC BY) license.

1. Introduction

Titanium mesh is widely used in oral and maxillofacial surgery for guided bone regeneration (GBR) and combined soft–hard tissue reconstruction due to its excellent mechanical stability, space-maintaining ability, and biocompatibility [1,2]. Successful GBR requires that the bone-facing side supports osteogenic cell migration and bone formation, while the soft-tissue side develops rapid and stable epithelial closure that prevents bacterial invasion [3–5]. However, synchronizing soft- and hard-tissue healing remains clinically challenging. Fibroblasts proliferate significantly faster than osteogenic cells, and soft-tissue overgrowth across mesh edges or perforations can block osteogenesis, reduce the achievable bone height, and greatly increase the risk of membrane exposure or graft failure [6,7].

Controlling fibroblast adhesion and migration on the soft-tissue side of titanium mesh is therefore essential for improving GBR outcomes [8]. Surface microtopography

engineering has emerged as an effective strategy for regulating cell behavior through biophysical cues [9–11]. Femtosecond-laser micro/nanoprocessing is particularly attractive due to its high precision, minimal thermal damage, and ability to generate consistent microstructures such as grooves, ridges, and hierarchical patterns [12,13]. Prior studies have shown that groove period, depth, and aspect ratio can modulate cell orientation, cytoskeletal tension, and proliferation [14].

Despite these above advances, there are still some issues: first, current designs primarily aim to promote cell adhesion, but the GBR's demands go far beyond it, which requires a combination of accelerated soft-tissue sealing and simultaneous suppression of unwanted fibroblast migration toward the bone side [15–17]. Second, the difference of periodic microstructures regulating fibroblast growth speed has rarely been studied, which is a critical determinant of soft-tissue overgrowth [18,19]. Third, it remains unclear whether two opposite functions, promotion and inhibition, can be integrated onto one surface and whether cells will exhibit purely geometry-driven spatial selectivity [20].

To meet such requirements, two femtosecond-laser–induced periodic stripe microstructures with distinct periods were fabricated on Ti surfaces, which are LIPSS and micro-ridges, which were formed through the interference between the incident field and surface-scattered waves or excited surface plasmon polaritons (SPPs). Results demonstrate that the two structures elicit sharply contrasting fibroblast responses and that their combination yields strong spatial selectivity, enabling a dual-function design capable of both promoting soft-tissue sealing and preventing peripheral overgrowth.

2. Materials and Methods

2.1. Femtosecond-Laser Fabrication of Stripe Microstructures

This experiment uses medical-grade pure titanium for making oral titanium mesh. Two types of stripe microstructure samples, LIPSS and micro-ridges, were fabricated using a Yb-solid-state femtosecond laser (Pharos, Light Conversion, Vilnius, Lithuania) with 230 fs, 1030 nm pulses. The Gaussian beam diameter was approximately 35 μm, and processing was conducted at normal incidence in ambient air.

Laser processing parameters were as follows. For LIPSS, the laser fluence was 3.54 J/cm^2, the repetition rate was 200 kHz, and the scanning speed was 2000 mm/s, with a scan-track spacing of 15 μm. For micro-ridges, the laser fluence was 5.66 J/cm^2, the repetition rate was 100 kHz, and the scanning speed was 1000 mm/s, with a scan-track spacing of 20 μm. Other processing conditions (wavelength 1030 nm, pulse duration 230 fs, spot diameter ~35 μm, and normal incidence in air) were identical. After laser structuring, samples were ultrasonically cleaned in ethanol.

2.2. Surface Characterization

Surface morphology of the samples was observed using field-emission scanning electron microscopy (FE-SEM, Quanta 450 FEG, FEI, Hillsboro, OR, USA). Surface chemical composition was characterized by X-ray photoelectron spectroscopy (XPS, Thermo ESCALAB 250XI). Vickers microhardness was measured with a FVM-800 microhardness tester (Vickers diamond indenter; Future-Tech, Izumi, Japan). Surface wettability was measured under ambient conditions using an OCA15EC system (DataPhysics, Filderstadt, Germany). The static water contact angle (WCA) was measured with an automated pipetting system, depositing 5 μL of Hanks' Balanced Salt Solution (HBSS) on the sample surface at room temperature.

2.3. Cell Culture and Seeding

The human gingival fibroblast cell line HGF-1 (ATCC CRL-2014, RRID: CVCL_3710) was used to evaluate the soft-tissue cytocompatibility of the laser-modified titanium surfaces. This cell line was obtained from the American Type Culture Collection (ATCC) and is widely used as a representative model for assessing gingival soft-tissue responses in implant-related studies. Routine screening confirmed that all cultures were free of mycoplasma contamination throughout the experiments. HGF-1 cells were expanded in Dulbecco's Modified Eagle's Medium (DMEM) supplemented with 10% fetal bovine serum (FBS). Cultures were maintained at 37 °C in a humidified incubator with 5% CO_2. This well-characterized fibroblast model ensures biologically relevant and reproducible results and supports the validity of conclusions regarding the soft-tissue cytocompatibility of the engineered microstructured surfaces.

Titanium specimens were sterilized under UV irradiation for 24 h before cell seeding. HGF-1 cells were seeded at a density of 7×10^4 cells by depositing 70 µL of the cell suspension directly onto each specimen placed in a 24-well plate. Cell viability was assessed using the CCK-8 assay following the manufacturer's instructions. Absorbance was measured at 450 nm using a microplate reader. For morphology evaluation, samples were rinsed three times in phosphate-buffered saline (PBS), fixed in 4% paraformaldehyde for 30 min, washed again in PBS, dehydrated through graded ethanol series, vacuum-dried, sputter-coated with gold, and imaged by scanning electron microscopy (SEM).

This procedure enabled detailed assessment of early fibroblast adhesion, spreading, and interaction with the laser-induced microstructures.

2.4. Statistical Analysis

For all cell experiments, three independent samples were tested for each group, with three technical replicates per sample. Data are presented as mean ± standard deviation. Statistical significance was determined using one-way ANOVA followed by Tukey's post hoc test when applicable. A value of * $p < 0.01$ was considered statistically significant.

2.5. Cells Live/Dead Staining

The cells on the samples are stained by a LIVE/DEAD BacLight Viability Kit (L-7012 LIVE/DEAD BacLight Bacterial Viability Kit, Thermo Fisher Scientific, Waltham, MA, USA) according to the instruction and observed by an epifluorescence microscope (TE2000-S2, Nikon, Tokyo, Japan).

3. Results and Discussion

Figure 1 illustrates the fabrication principle and structural characteristics of the two femtosecond-laser–induced stripe microstructures produced on Ti substrates. Both LIPSS and micro-ridges patterns were generated under an identical unidirectional scanning strategy, with laser fluence and scan-track spacing serving as the only tuning parameters. The schematic highlights pulse-overlap behavior, the LIPSS formation mechanism, and the resulting geometric parameters of each pattern. Quantitative comparison shows that LIPSS exhibits fine, densely packed subwavelength ripples, whereas micro-ridges display markedly larger periods and wider grooves, demonstrating highly reproducible topographical modulation through controlled energy–spacing interactions. These results confirm that the two microstructures originate strictly from tunable LIPSS mechanisms, establishing a clear geometric foundation for all subsequent biological assays.

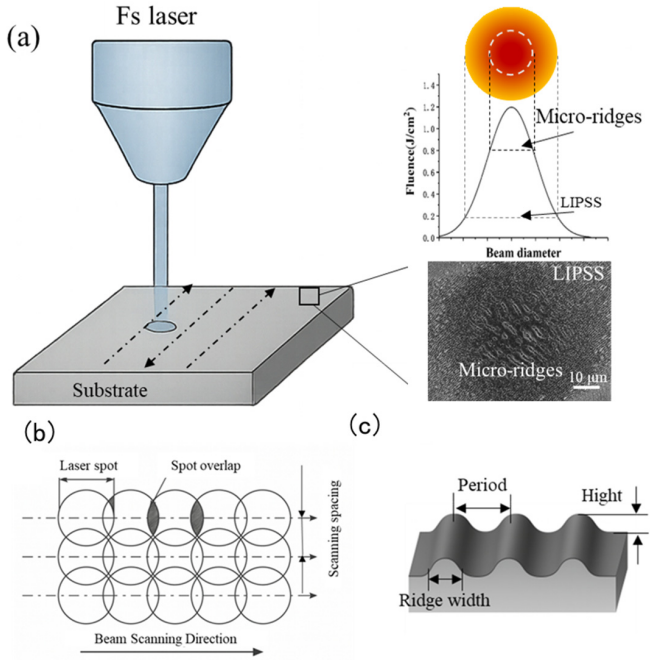
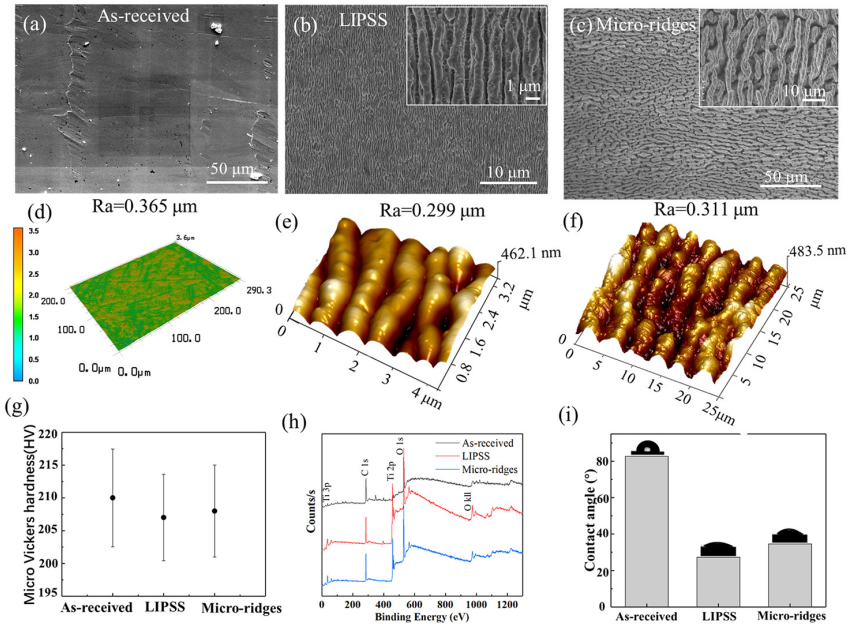


Figure 1. Femtosecond-laser fabrication of dual-period stripe microstructures on Ti substrates: (**a**) Schematic of ultrafast pulse interaction with Ti surface; (**b**) Unidirectional scanning strategy and pulse-overlap configuration; (**c**) Schematic diagram of geometric dimensions of stripes.

Figure 2 shows the morphological and physicochemical characterization of the untreated Ti surface and the two laser-induced microstructures. SEM and AFM clearly reveal that femtosecond-laser processing generates periodic ripples with distinct geometries: LIPSS exhibits a small period (820 ± 30 nm), narrow ridge width (624 ± 30 nm), and shallow height (210 ± 20 nm), whereas micro-ridges present a much larger period (4.7 ± 0.1 μm), wider ridges (2.2 ± 0.1 μm), and comparable height (220 ± 20 nm). Although they exhibit notable structural contrasts, all of the surfaces display near-equal roughness values of Ra = 0.365, 0.299 and 0.311 μm. Although the arithmetic roughness (Ra) values are comparable among all groups, the densely packed submicron features may increase the effective surface area at the micro/nanoscale, which can partially contribute to the enhanced early cell adhesion and spreading. Used for identical XPS compositions with only minimal differences in microhardness and wettability, these results verify that LIPSS and micro-ridges vary only topographically without any difference chemically so that no biological effects arise. Responses appearing afterwards are dependent on geometry and not chemistry or mechanics.

Fibroblasts adhered and spread after 24 h on the untreated Ti, LIPSS, and micro-ridges surfaces are shown in Figure 3. The microstructure possessed a fine submicron period (820 ± 30 nm) and narrower ridge width (624 ± 30 nm), and these features exhibited elongated morphology and proper alignment. Actin fibers align with the ripple direction showing strong contraction ability. Unlike the contact-guidance cues, which favor tissue adhering, the micro-ridges surface with a period of 4.7 ± 0.1 μm and groove width of 2.2 ± 0.1 μm encourages adherence of small, round, disorganized cells, indicating poor adhesion stability. On the other hand, the untreated Ti surface shows medium and irregular spreading behavior. High-magnification SEM further confirms abundant lamellipodia and cytoskeletal extensions on LIPSS as shown in Figure 3, whereas micro-ridges have less lamellipodia/cytoskeletal protrusions. These results demonstrate that the fine, densely packed LIPSS ripples can promote cytoskeletal organization and early adhesion, while the course, widely spaced micro-ridges grooves disrupt stable anchoring. The microstructure–cell interaction observed here directly reflects the size-dependent topographical cues identified

in Figure 2 and lays the mechanobiological foundation for the differential proliferation and spatial selectivity observed in subsequent figures.



Mircrostructural dimensions: LIPSS: period=820±30 nm; ridge width=624±30 nm; height=210±20 nm; Micro-ridges: period=4.7±0.1 μm; ridge width= 2.2±0.1 μm; height=220±20 nm.

Figure 2. Morphological and physicochemical characteristics of untreated Ti, LIPSS, and micro-ridges surfaces: (**a**–**c**) SEM morphology; (**d**–**f**) AFM 3D topography and groove-dimension quantification; (**g**) Microhardness comparison; (**h**) XPS spectra; (**i**) Water contact angle.

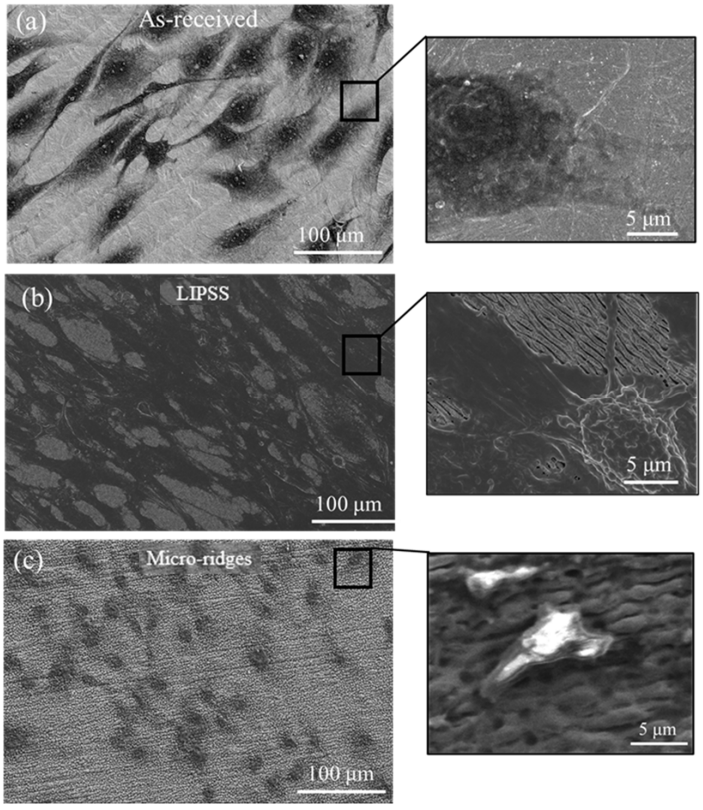


Figure 3. Fibroblast adhesion and early cytoskeletal organization on three surfaces after 24 h: (**a**–**c**) Low-magnification and high-magnification SEM showing overall adhesion on Ti, LIPSS, and micro-ridges.

Figure 4 illustrates fibroblast proliferation and cytoskeletal organization on the three surfaces at 24 and 48 h, revealing a pronounced geometry-dependent divergence consistent with the structural characteristics described in Figure 2. The submicron micro-ridges pattern (periodicity ~820 nm and ridge width ~620 nm) supports dense actin filament organization and significantly higher cell densities at both time points. In contrast, the micro-groove structure (periodicity ~4.7 μm and groove width ~2.2 μm) maintains sparse cell populations with poorly developed cytoskeletal networks.

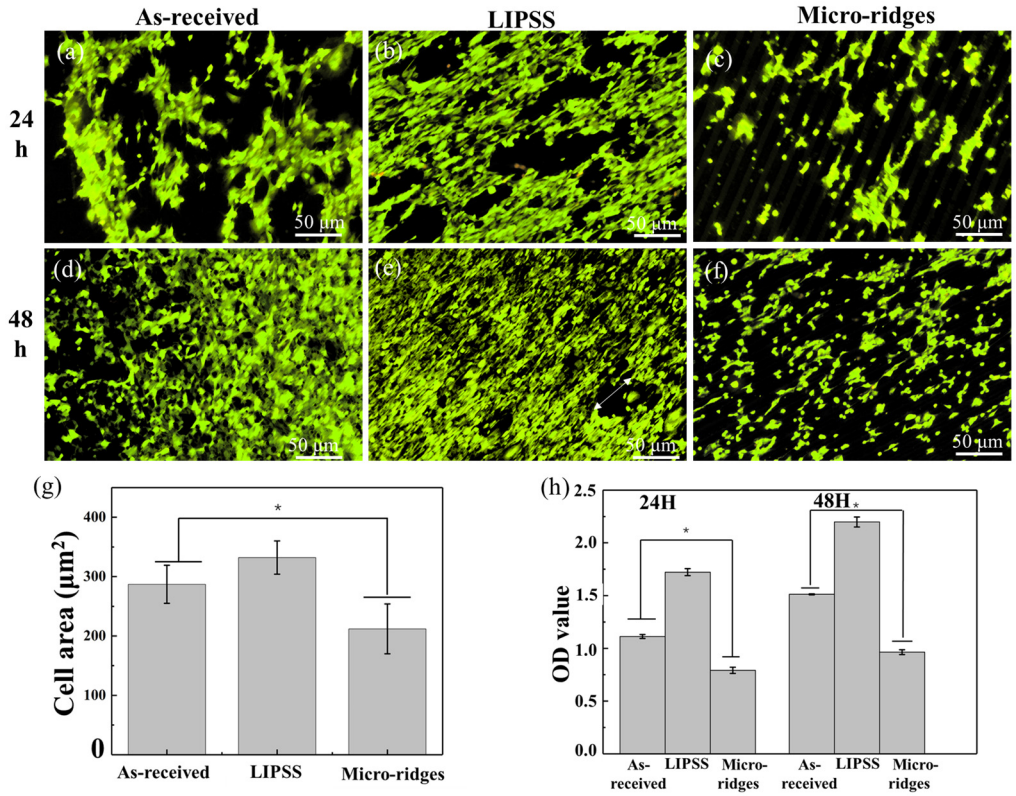


Figure 4. Geometry-dependent proliferation and spreading of fibroblasts at 24 and 48 h: (**a**–**c**) Fluorescence images of cells on Ti, LIPSS, and micro-ridges at 24 h; (**d**–**f**) Fluorescence images at 48 h; (**g**) Quantitative spreading-area analysis; (**h**) CCK-8 metabolic activity (OD) at 24 and 48 h. * $p < 0.01$.

Results of the quantitative spreading-area analysis further confirm significantly larger cellular footprints on micro-ridges surfaces, whereas markedly restricted spreading is observed on the micro-grooved surfaces. Despite similar Ra values, the densely packed submicron ripples are likely to generate a higher effective surface area than the more widely spaced microstructures. This increase may modulate the amount and spatial distribution of adsorbed proteins, thereby providing more potential anchoring sites for integrin engagement and ultimately influencing early cell adhesion and spreading.

Importantly, since surface chemistry, wettability, and bulk mechanical properties remain nearly unchanged across the groups, and given that the micro-groove structure exhibits larger geometric dimensions despite similar roughness values, the observed biological differences are more reasonably attributed to geometry-dependent topographical cues rather than to chemical or roughness-related factors. Protein adsorption serves as a critical intermediate mechanism linking surface properties to cellular responses. Topography-induced variations in the amount and conformation of adsorbed proteins (e.g., fibronectin- or vitronectin-mediated integrin binding) may modulate focal adhesion assembly and cytoskeletal organization, thereby influencing fibroblast attachment and proliferation on the patterned titanium substrates.

Figure 5 illustrates the geometry-driven spatial selective adhesion on alternating LIPSS–micro-ridges arrangements, further validating the size-dependent topographical cues established earlier. In both the parallel and cross-shaped patterns with 10 μm spacing, fibroblasts preferentially populate LIPSS regions composed of 820 nm ripples, while distinctly avoiding micro-ridges regions with 4.7 μm coarse grooves. SEM and magnified insets show elongated, aligned cells on LIPSS stripes, contrasted by rounded, poorly attached cells on micro-ridges stripes. This confirms that submicron-scale features favor stable cytoskeletal anchoring, whereas micron-scale grooves interrupt focal adhesion formation and hinder lamellipodia extension. Importantly, this spatial sorting occurs without any biochemical cues, demonstrating that microstructure dimensionality alone provides sufficient contrast to drive deterministic cell positioning. This figure establishes that the bidirectional regulatory capacity of LIPSS and micro-ridges can be seamlessly integrated into patterned designs, enabling engineered "promoting islands" and "inhibitory rings" for soft-tissue control.

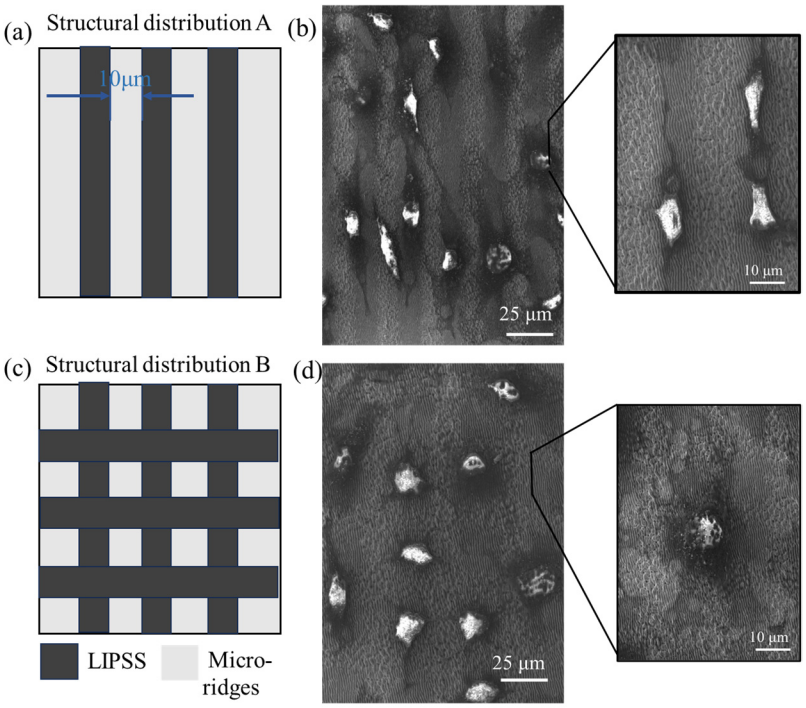


Figure 5. Spatially selective adhesion on alternating LIPSS–micro-ridges patterned surfaces: (**a**) Parallel alternating microstructure layout (10 μm spacing); (**b**) SEM showing preferential adhesion to LIPSS stripes; (**c**) Cross-grid alternating layout (10 μm spacing); (**d**) SEM and magnified views highlighting selective occupancy of LIPSS regions.

Figure 6 converts the different dimensions of LIPSS and micro-ridges into two functions for titanium mesh implants in the GBR. In the soft-tissue–facing side, LIPSS is placed at the center location taking advantage of its fine periodicity of 820 nm to better improve the adhesion of fibroblasts and epithelial rapid sealing compared with that of micro-ridges. Inhibitory rings, characterized by a broad 4.7 μm period, are placed all over the mesh pores so as to prevent downward movement to the bone side of the pore. The biological diagram shows that fibroblasts can spread easily, moving across LIPSS areas but being blocked and impeded at the micro-ridges areas. They associate with boundaries in which the larger groove impairs cytoskeletal anchoring, reducing cell spreading and limiting cytoskeletal anchoring at the micro-groove regions. Moreover, as pointed out, both LIPSS and micro-ridges originate from femtosecond-laser–induced periodic surface. Patterning the two micro-zones onto the titanium mesh using high spatial accuracy can be accomplished easily

just by changing the laser fluence scanning interval, without modification of materials and without adding extra processes. This purely physical, maskless, and reproducible approach aligns well with clinical manufacturing workflows and minimizes concerns about long-term chemical degradation or foreign agent release. This geometry-driven segregation mirrors the mechanobiological behaviors that can be observed in Figures 3–5, which provides a translational strategy to overcome the long-standing challenge of soft-tissue overgrowth through titanium mesh pores.

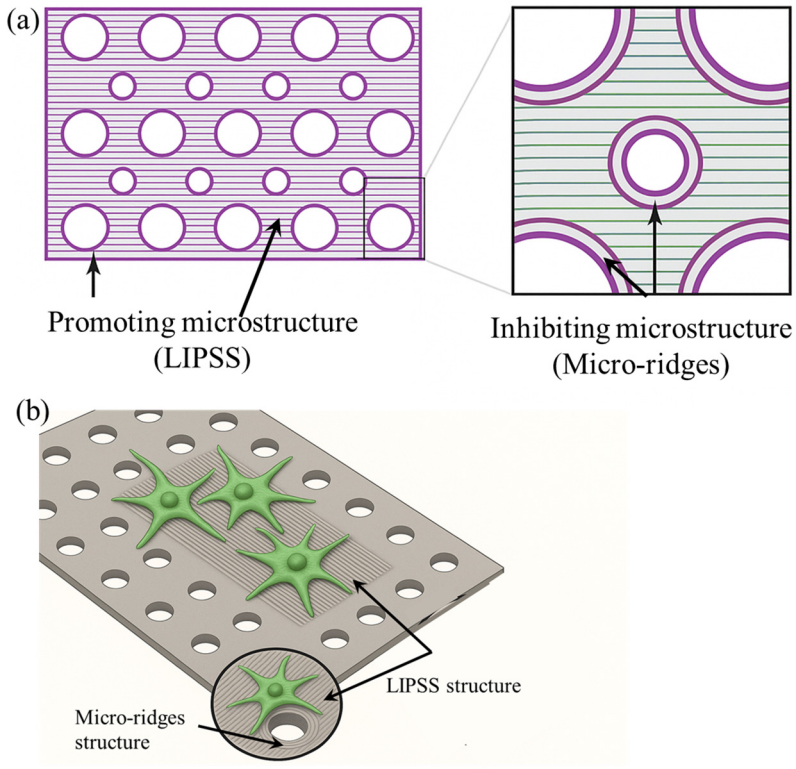


Figure 6. Schematic illustration of the dual-function microtopographic interface for soft-tissue regulation on titanium mesh implants: (**a**) LIPSS-based promoting regions and micro-ridges inhibitory rings arranged on the soft-tissue–facing side of a perforated mesh; (**b**) Mechanobiological schematic showing rapid spreading on LIPSS zones and suppressed downward migration at micro-ridges boundaries.

4. Conclusions

This study demonstrates that femtosecond-laser–induced stripe microstructures with distinct periodicities can bidirectionally regulate fibroblast behavior through purely physical topographical cues. Submicron LSFL promotes cell adhesion, spreading, and proliferation, whereas micron-scale micro-grooves restrict these processes by limiting stable cytoskeletal organization. When integrated on a single surface, these geometrical contrasts generate clear spatial selectivity without altering surface chemistry. Beyond direct geometrical guidance, protein adsorption likely acts as a key intermediate mechanism. Geometry-dependent variations in protein amount and conformation may modulate integrin engagement and focal adhesion assembly, thereby contributing to the observed differences in cellular response. Owing to the shared femtosecond-laser fabrication principle, both structures can be precisely patterned through simple parameter adjustment, enabling a dual-function interface design. Collectively, this work provides a fabrication-ready and mechanistically grounded surface-engineering strategy to enhance soft-tissue control and improve predictability in guided bone regeneration.

Future work should focus on in vivo validation and long-term biological evaluation under clinically relevant conditions. In addition, optimization of laser parameters for large-area manufacturing, assessment of durability under oral mechanical/chemical challenges, and evaluation of soft–hard tissue outcomes in relevant models will be essential to facilitate clinical translation of this surface-engineering strategy.

Author Contributions: Conceptualization, L.L.; methodology, J.Z. and T.Y.; investigation, J.Z.; resources, T.Y.; data curation, X.Z.; writing—original draft preparation, J.Z. and J.Y.; writing—review and editing, L.L.; supervision, L.L.; funding acquisition, J.Z. and L.L. All authors have read and agreed to the published version of the manuscript.

Funding: This research was funded by the Natural Science Foundation of Ningbo (2024J098), Ningbo University of Technology Research Cultivation Program (2022TS16), Ningbo University of Technology Research Startup Fund (2022KQ16), International Sci-tech Cooperation Projects under the "Innovation Yongjiang 2035" Key R&D Programme (2024H014), Ningbo Yongjiang Young talent sub-project Programme (2022A-147-G), and Ningbo "Innovation Yongjiang 2035" Key R&D Programme (2025Z075).

Institutional Review Board Statement: Not applicable.

Informed Consent Statement: Not applicable.

Data Availability Statement: Data are contained within the article.

Conflicts of Interest: Authors Xinran Zhang and Jin Yang were employed by the Ningbo Hangzhou Bay Branch, Zhejiang Jirun Automobile Co., Ltd. The remaining authors declare that the research was conducted in the absence of any commercial or financial relationships that could be construed as a potential conflict of interest.

Abbreviations

The following abbreviations are used in this manuscript:

GBR	guided bone regeneration
LIPSS	laser-induced periodic surface structures
SPPs	surface plasmon polaritons

References

1. Alazmi, S.O. A Review on Guided Bone Regeneration Using Titanium Mesh. *Bioinformation* **2024**, *20*, 562–565. [CrossRef] [PubMed]
2. Mateo-Sidrón Antón, M.C.; Pérez-González, F.; Meniz-García, C. Titanium Mesh for Guided Bone Regeneration: A Systematic Review. *Br. J. Oral Maxillofac. Surg.* **2024**, *62*, 433–440. [CrossRef] [PubMed]
3. Hartmann, A.; Seiler, M. Minimizing Risk of Customized Titanium Mesh Exposures—A Retrospective Analysis. *BMC Oral Health* **2020**, *20*, 36. [CrossRef] [PubMed]
4. Gu, C.; Xu, L.; Shi, A.; Guo, L.; Chen, H.; Qin, H. Titanium Mesh Exposure in Guided Bone Regeneration Procedures: A Systematic Review and Meta-Analysis. *Int. J. Oral Maxillofac. Implant.* **2022**, *37*, e29–e40. [CrossRef] [PubMed]
5. Xie, Y.; Li, S.; Zhang, T.; Wang, C.; Cai, X. Titanium Mesh for Bone Augmentation in Oral Implantology: Current Application and Progress. *Int. J. Oral Sci.* **2020**, *12*, 37. [CrossRef] [PubMed]
6. Milillo, L.; Petruzzi, M. Guided Bone Regeneration with Occlusive Titanium Barrier: A Case Report and Clinical Considerations. *Biomimetics* **2023**, *8*, 106. [CrossRef] [PubMed]
7. Wang, S.; Zhang, M.; Liu, L.; Xu, R.; Huang, Z.; Shi, Z.; Liu, J.; Li, Z.; Li, X.; Hao, P.; et al. Femtosecond Laser Treatment Promotes the Surface Bioactivity and Bone Ingrowth of Ti6Al4V Bone Scaffolds. *Front. Bioeng. Biotechnol.* **2022**, *10*, 962483. [CrossRef] [PubMed]
8. Madapana, D.; Bathe, R.; Manna, I.; Majumdar, J.D. Laser Surface Structuring of Titanium Alloy (Ti-6Al-4V) for Improved Tribocorrosion Resistance for Bio-Implant Applications. *Tribol. Int.* **2024**, *197*, 109711. [CrossRef]
9. Zhang, Q.; Guan, Y. Laser Induced Periodic Surface Structure on Titanium Alloy and Its Effect on Microstructure Refinement and Corrosion Behavior. *J. Alloys Compd.* **2023**, *936*, 168188. [CrossRef]

10. Martínez-Calderon, M.; Martín-Palma, R.J.; Rodríguez, A.; Gómez-Aranzadi, M.; García-Ruiz, J.P.; Olaizola, S.M.; Manso-Silván, M. Biomimetic Hierarchical Micro/Nano Texturing of TiAlV Alloys by Femtosecond Laser Processing for the Control of Cell Adhesion and Migration. *Phys. Rev. Mater.* **2020**, *4*, 056008. [CrossRef]
11. Vorobyev, A.Y.; Guo, C. Femtosecond Laser Structuring of Titanium Implants. *Appl. Surf. Sci.* **2007**, *253*, 7272–7280. [CrossRef]
12. Erdoğan, M.; Öktem, B.; Kalaycıoğlu, H.; Yavaş, S.; Mukhopadhyay, P.K.; Eken, K.; Özgören, K.; Aykaç, Y.; Tazebay, U.H.; Ilday, F.Ö. Texturing of Titanium (Ti6Al4V) Medical Implant Surfaces with MHz-Repetition-Rate Femtosecond and Picosecond Yb-Doped Fiber Lasers. *Opt. Express* **2011**, *19*, 10986. [CrossRef] [PubMed]
13. Bonse, J.; Gräf, S. Maxwell Meets Marangoni—A Review of Theories on Laser-Induced Periodic Surface Structures. *Laser Photonics Rev.* **2020**, *14*, 2000215. [CrossRef]
14. Zhang, Y.; Jiang, Q.; Long, M.; Han, R.; Cao, K.; Zhang, S.; Feng, D.; Jia, T.; Sun, Z.; Qiu, J.; et al. Femtosecond Laser-Induced Periodic Structures: Mechanisms, Techniques, and Applications. *OES* **2022**, *1*, 220005. [CrossRef]
15. Arora, S.; Lin, S.; Cheung, C.; Yim, E.K.F.; Toh, Y.-C. Topography Elicits Distinct Phenotypes and Functions in Human Primary and Stem Cell Derived Endothelial Cells. *Biomaterials* **2020**, *234*, 119747. [CrossRef] [PubMed]
16. Azatov, M.; Sun, X.; Suberi, A.; Fourkas, J.T.; Upadhyaya, A. Topography on a Subcellular Scale Modulates Cellular Adhesions and Actin Stress Fiber Dynamics in Tumor Associated Fibroblasts. *Phys. Biol.* **2017**, *14*, 065003. [CrossRef] [PubMed]
17. Kim, D.-H.; Han, K.; Gupta, K.; Kwon, K.W.; Suh, K.-Y.; Levchenko, A. Mechanosensitivity of Fibroblast Cell Shape and Movement to Anisotropic Substratum Topography Gradients. *Biomaterials* **2009**, *30*, 5433–5444. [CrossRef] [PubMed]
18. Uttayarat, P.; Chen, M.; Li, M.; Allen, F.D.; Composto, R.J.; Lelkes, P.I. Microtopography and Flow Modulate the Direction of Endothelial Cell Migration. *Am. J. Physiol.-Heart Circ. Physiol.* **2008**, *294*, H1027–H1035. [CrossRef]
19. Riveiro, A.; Maçon, A.L.B.; Del Val, J.; Comesaña, R.; Pou, J. Laser Surface Texturing of Polymers for Biomedical Applications. *Front. Phys.* **2018**, *6*, 16. [CrossRef]
20. Cholkar, A.; McCann, R.; Kinahan, D.; Brabazon, D. Ultrafast Laser-Induced Surface Structuring of Anti-Fouling Steel Surfaces for Biomedical Applications. In *Volume 1: Additive Manufacturing; Biomanufacturing; Life Cycle Engineering; Manufacturing Equipment and Automation; Nano/Micro/Meso Manufacturing*; American Society of Mechanical Engineers: New York, NY, USA, 2022; p. V001T07A008.

Disclaimer/Publisher's Note: The statements, opinions and data contained in all publications are solely those of the individual author(s) and contributor(s) and not of MDPI and/or the editor(s). MDPI and/or the editor(s) disclaim responsibility for any injury to people or property resulting from any ideas, methods, instructions or products referred to in the content.